Oxidative addition to main group versus transition metals: Insights from the Activation Strain model

G. Theodoor de Jong, Ruud Visser, F. Matthias Bickelhaupt *

Afdeling Theoretische Chemie, Scheikundig Laboratorium der Vrije Universiteit, De Boelelaan 1083, NL-1081 HV Amsterdam, The Netherlands

Abstract

We have studied the oxidative addition of the methane C–H and chloromethane C–Cl bonds to a number of main group (Be, Mg and Ca) and transition metals (Pd, Zn and Cd), using relativistic density functional theory (DFT) at ZORA-BLYP/TZ2P. The purpose is to better understand what causes the characteristic differences in reactivity between main group and transition metals towards oxidative addition. Thus, we have analyzed our model reactions using the Activation Strain model in which the activation energy $\Delta E^{\neq}$ is decomposed into the activation strain $\Delta E^{\neq}_{strain}$ of and the stabilizing TS interaction $\Delta E^{\neq}_{int}$ between the reactants in the activated complex: $\Delta E^{\neq} = \Delta E^{\neq}_{strain} + \Delta E^{\neq}_{int}$. Activation of the C–H bond goes with higher barriers than activation of the C–Cl bond because the higher bond strength of the former translates into a higher activation strain $\Delta E^{\neq}_{strain}$. The barriers for bond activation increase along Pd < Be, Ca < Mg < Zn, Cd. This can be straightforwardly understood through the TS-interaction $\Delta E^{\neq}_{int}$, that is, in terms of the bonding capabilities of the metals. Pd yields the lowest barriers because it achieves the most stabilizing $\Delta E^{\neq}_{int}$. This is the result of the small HOMO–LUMO gap between its occupied 4d and unfilled 5s AOs, which makes Pd both a good electron donor and acceptor. Zn and Cd yield the highest barriers because the large HOMO–LUMO gap between the occupied valence ns and unfilled valence np AOs makes them both poor donors and poor acceptors of electronic charge.
© 2006 Elsevier B.V. All rights reserved.

Keywords: Activation Strain model; Bond activation; Oxidative addition; Catalysis; Density functional calculations; Alkaline earths; Transition metals

1. Introduction

Oxidative addition and reductive elimination (Eq. (1)) are key steps in many reactions of homogeneous catalysis [1,2] and have been intensively investigated both experimentally [2–4] and theoretically [4–10]

$$\text{ML}_n + \text{R–X} \underset{\text{Reductive Elimination}}{\overset{\text{Oxidative Addition}}{\rightleftharpoons}} \text{R–ML}_n\text{–X} \qquad (1)$$
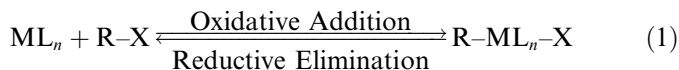
A well-known class of processes involving oxidative addition is catalytic C–X bond activation [11–13]. The catalytically active species in these reactions are generally coordination complexes of palladium or other transition-metals. Main-group metals do have a rich chemistry [12–15] but they a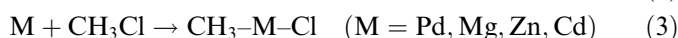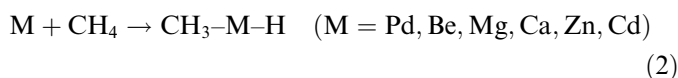re commonly not involved in catalytic bond activation through oxidative insertion. An exception is carbon–halogen bond activation by ground-state magnesium through matrix deposition, which yields Grignard's reagent RMgX [12,13,15,16].

In the present study, we aim at obtaining more insight into *why* transition metals are better agents for oxidative insertion than main-group metals such as alkaline earths. Oxidative insertion of a metal into a C–X bond is associated with increasing the oxidation state of the metal atom by +2. The particular capability of transition metals to undergo such reactions has been ascribed, amongst others, to the ease with which they can change their oxidation state [12]. In a sense, however, this is a reformulation of the question rather than an answer. Here, we make an attempt to trace the characteristic difference in reactivity between transition and main-group metals to corresponding characteristic features in their orbital electronic structure. To this end, a detailed study of the reactivity of a series of

* Corresponding author. Fax: +31 20 59 87629.
E-mail address: fm.bickelhaupt@few.vu.nl (F.M. Bickelhaupt).

transition and main-group metals towards the methane C–H and chloromethane C–Cl bonds has been carried out using relativistic nonlocal density functional theory (DFT) at the ZORA-BLYP/TZ2P level (see Section 2). This approach was previously shown to agree excellently with highly correlated ab initio benchmark studies for describing the insertion of palladium into C–H, C–Cl and other bonds [8–10]. Our investigation covers the transition metal Pd and the alkaline earth metals Be, Mg and Ca. Furthermore, we have included the group-12 transition metals Zn and Cd, the behavior of which is known to resemble, to some extent, that of the alkaline earths [12,14]. Thus, all together, the potential energy surfaces (PES) of the following model reactions (Eqs. (2) and (3)) were explored and compared:

$$M + CH_4 \rightarrow CH_3-M-H \quad (M = Pd, Be, Mg, Ca, Zn, Cd) \tag{2}$$

$$M + CH_3Cl \rightarrow CH_3-M-Cl \quad (M = Pd, Mg, Zn, Cd) \tag{3}$$

These model reactions reveal the *intrinsic* characteristics of and differences between the categories of metals, that is, their behavior in the absence of solvent molecules and ligands. While the latter may substantially affect the precise shape of PESs for real condensed-phase reactions, our study suggests that essential aspects of their behavior are inherited from this intrinsic nature of the metal atoms.

The difference in reactivity for the various combinations of inserting metals and bonds is analyzed and interpreted in terms of the Activation Strain model of chemical reactivity [6,7,17]. In this model, activation energies $\Delta E^{\neq}$ are decomposed into the activation strain $\Delta E^{\neq}_{strain}$ of and the stabilizing transition state (TS) interaction $\Delta E^{\neq}_{int}$ between the reactants in the activated complex: $\Delta E^{\neq} = \Delta E^{\neq}_{strain} + \Delta E^{\neq}_{int}$. The activation strain $\Delta E^{\neq}_{strain}$ depends on the strength of the activated bond and on the extent to which a particular metal expands the bond in the activated complex. The TS interaction $\Delta E^{\neq}_{int}$ is directly determined by the bonding capabilities and, thus, the frontier orbitals of the reactants. As will emerge from our analyses, much of the characteristics of Pd versus alkaline earths versus group-12 metals can be traced to the respective valence configurations: s^0d^{10}, s^2d^0 and s^2d^{10}, respectively. In practice, of course, catalytic activity and selectivity of *solution-phase* transition or main-group metal *complexes* are substantially affected by coordination of ligands and interaction with solvent molecules. However, the starting point in this pilot study is the investigation of the *intrinsic* reactivity of the transition metal *atom*.

2. Methods

2.1. Computational details

All calculations are based on density functional theory (DFT) [18], using the Amsterdam Density Functional (ADF) program [19,20]. The BLYP density functional was used

[21], in combination with a large uncontracted set of Slater-type orbitals (STOs) containing diffuse functions. This basis set is designated TZ2P: it is of triple-ζ quality and has been augmented with two sets of polarization functions on each atom. The core shells of carbon (1s), chlorine (1s2s2p), beryllium (1s), magnesium (1s), calcium (1s2s2p), zinc (1s2s2p), palladium (1s2s2p3s3p3d), and cadmium (1s2s2p3s3p3d) were treated by the frozen-core approximation [19]. An auxiliary set of s, p, d, f and g STOs was used to fit the molecular density and to represent the Coulomb and exchange potentials accurately in each SCF cycle [19]. Relativistic effects were accounted for using the zeroth-order regular approximation (ZORA) [22]. This computational approach was shown to be in good agreement with high-level ab initio calculations for oxidative addition reactions to Pd [8–10].

Equilibrium and transition state geometries were fully optimized using analytical gradient techniques. All structures were verified by frequency calculations: for minima all normal modes have real frequencies, whereas transition states have one normal mode with an imaginary frequency. The character of the normal mode associated with the imaginary frequency was analyzed to ensure that the correct transition state was found.

2.2. Activation Strain analyses

To gain insight into how the use of different metals and different substrates affects the activation barriers of the different oxidative insertion reactions, i.e., insight into how this effect depends on the nature of the concomitant geometrical deformation and electronic structure of reacting metal and substrate, the reactions were analyzed using the Activation Strain model of chemical reactivity [6,7,17]. In this model, the activation energy $\Delta E^{\neq}$ is decomposed into the activation strain $\Delta E^{\neq}_{strain}$ and the transition state (TS) interaction $\Delta E^{\neq}_{int}$ (see Eq. (4) and Fig. 1):

$$\Delta E^{\neq} = \Delta E^{\neq}_{strain} + \Delta E^{\neq}_{int} \tag{4}$$

The activation strain $\Delta E^{\neq}_{strain}$ is the strain energy associated with deforming the reactants from their equilibrium geometry to the geometry they acquire in the activated complex (Fig. 1). The TS interaction $\Delta E^{\neq}_{int}$ is the actual interaction energy between the deformed reactants in the transition state. In the present study, one of the reactants is the neutral metal atom and the other reactant is one of the substrates CH_4 and CH_3Cl.

The TS interaction $\Delta E^{\neq}_{int}$ between the strained reactants is further analyzed in the conceptual framework provided by the Kohn–Sham molecular orbital (KS-MO) model [23]. To this end, it is further decomposed into three physically meaningful terms (Eq. (5)) using the extended transition state (ETS) method developed by Ziegler and Rauk [24]:

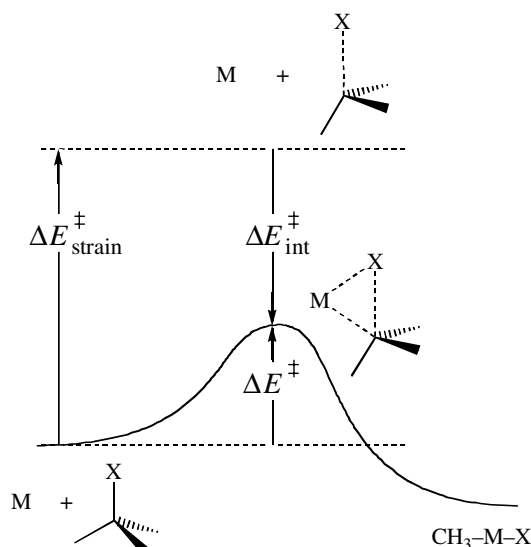$$\Delta E^{\neq}_{int} = \Delta V_{elst} + \Delta E_{Pauli} + \Delta E_{oi} \tag{5}$$

Fig. 1. Illustration of the Activation Strain model in case of oxidative insertion of a metal M into a C–X bond. The activation energy $\Delta E^{\neq}$ is decomposed into the activation strain $\Delta E^{\neq}_{strain}$ of and the stabilizing TS interaction $\Delta E^{\neq}_{int}$ between the reactants in the transition state.

The term ΔV_{elst} corresponds to the classical electrostatic interaction between the unperturbed charge distributions of the deformed reactants and is usually attractive. The Pauli repulsion ΔE_{Pauli} comprises the destabilizing interactions between occupied orbitals and is responsible for any steric repulsion. The orbital interaction ΔE_{oi} accounts for charge transfer (interaction between occupied orbitals on one moiety with unoccupied orbitals of the other, including the HOMO–LUMO interactions) and polarization (empty–occupied orbital mixing on one fragment due to the presence of another fragment).

3. Results and discussion

3.1. Reaction profiles and geometries

In this section, we discuss the potential energy surfaces (PESs) of the various oxidative insertion reactions as well as the geometries of stationary points along the reaction coordinate. The results are summarized in Figs. 2 and 3 (geometries), Fig. 4 (reaction profiles) and Table 1 (energies). The results of the Activation Strain analyses are discussed in Section 3.2.

The reactions of Pd + CH$_4$ and Pd + CH$_3$Cl have been reported before [8,10,25]. The latter, i.e., Pd + CH$_3$Cl, may also proceed via an alternative, higher-energy S$_N$2 pathway for the details of which the reader is referred to Refs. [10,25]. Here, we will focus on oxidative insertion.

All model reactions proceed from the reactants via a transition state (TS) to a product (P), see Figs. 2 and 3. The reactions of Pd involve, in addition, the formation of a stable reactant complex (RC) prior to advancing to the TS, see 2a and 9a in Figs. 2 and 3. For all other metals, such encounter complexes are essentially unbound and
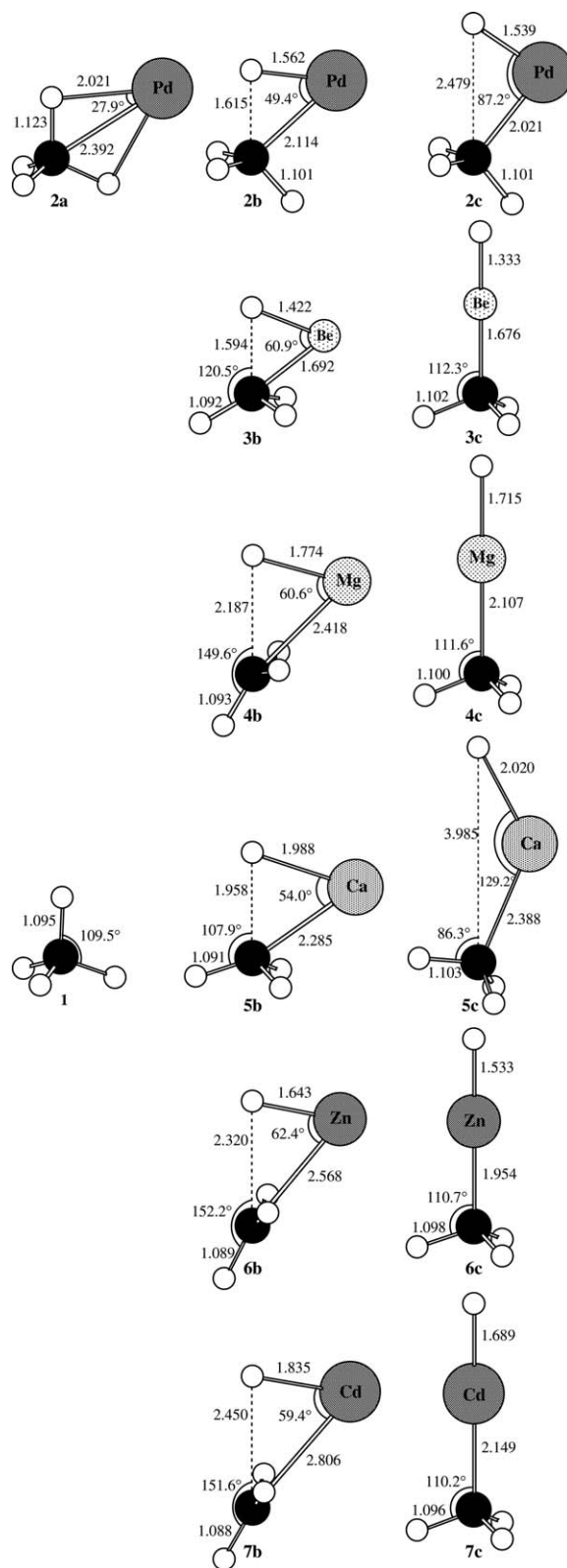

Fig. 2. Geometries (in Å, °) at ZORA-BLYP/TZ2P of stationary points along the potential energy surface for oxidative insertion of Pd, Be, Mg, Ca, Zn, and Cd into the C–H bond of CH$_4$.

thus not existent. Table 1 contains the energies relative to reactants of all stationary points along the potential energy surface. The activation and reaction energies are also
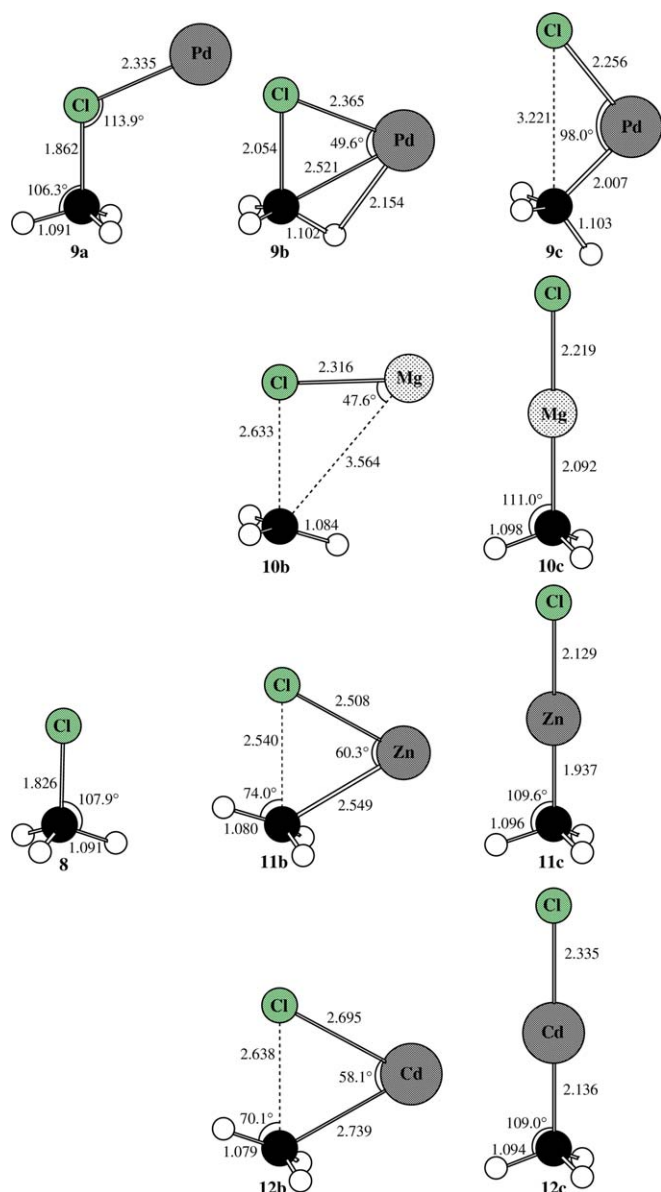
Fig. 3. Geometries (in Å, °) at ZORA-BLYP/TZ2P of stationary points along the potential energy surface for oxidative insertion of Pd, Mg, Zn, and Cd into the C–Cl bond of CH_3Cl.
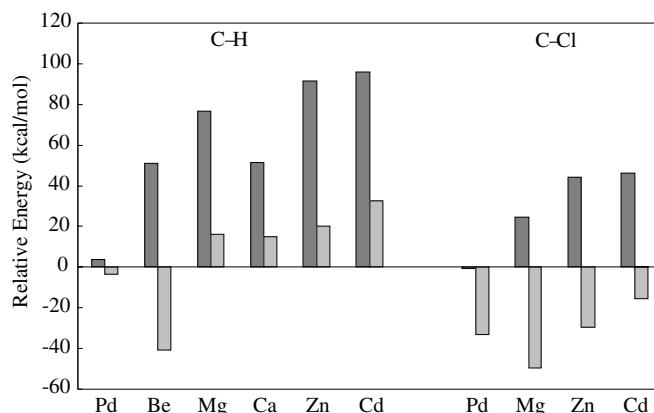

Fig. 4. Activation (left bars) and reaction (right bars) energies (in kcal/mol; relative to reactants) at ZORA-BLYP/TZ2P for the oxidative insertion reactions of Pd, Be, Mg, Ca, Zn and Cd with CH_4, and Pd, Mg, Zn and Cd with CH_3Cl.

Table 1
Reaction profiles (in kcal/mol; relative to reactants) for the oxidative insertion reactions of Pd, Be, Mg, Ca, Zn and Cd with CH_4, and Pd, Mg, Zn and Cd with CH_3Cl[a]

Activated bond	Reactants	Reactant complex	Transition state	Product
C–H	Pd + CH_4[b]	−6.7	3.9	−3.4
	Be + CH_4	[c]	51.0	−40.6
	Mg + CH_4	[c]	76.7	16.0
	Ca + CH_4	[c]	51.7	14.9
	Zn + CH_4	[c]	91.6	20.4
	Cd + CH_4	[c]	96.1	32.7
C–Cl	Pd + CH_3Cl[d]	−12.9	−0.6	−33.1
	Mg + CH_3Cl	[c]	24.6	−49.7
	Zn + CH_3Cl	[c]	44.3	−29.6
	Cd + CH_3Cl	[c]	46.0	−15.5

[a] Computed at ZORA-BLYP/TZ2P.
[b] From Ref. [8].
[c] RC unbound.
[d] From Ref. [10].

graphically represented in the bar diagram of Fig. 4. Two striking trends emerge: (i) the activation energies for insertion into the C–H bond are significantly higher than those for insertion into the C–Cl bond; (ii) activation energies increase roughly in the order Pd < alkaline earths < group 12 (or more precisely Pd < Be, Ca < Mg < Zn, Cd).

The activation energies for oxidative insertion into the C–H bond of methane (**1**) are between 4 and 96 kcal/mol and are significantly higher than those for oxidative insertion into the C–Cl bond of chloromethane (**2**) which range from −1 up to only 46 kcal/mol (see Table 1 and Fig. 3). The Activation Strain analysis of Section 3.2 will reveal that the lower barrier for insertion into the C–Cl bond is related to the fact that the C–Cl bond is weaker than the C–H bond. Insertion into the C–Cl bond is overall also sig-

nificantly more exothermic than insertion into the C–H bond (see Table 1 and Fig. 3). Most products have C_{3v} point-group symmetry with a linear C–M–H or C–M–Cl unit. Exceptions are the products of Pd + CH_4 (**2c**) and Pd + CH_3Cl (**9c**), which have C–Pd–H and C–Pd–Cl angles of 87° and 98°, respectively, and the product of Ca + CH_4 (**5c**), which has a C–Ca–H angle of 129°.

Next, we have a closer look at the activation energies and TS structures for oxidative insertion into the methane C–H bond and how they depend on the inserting metal atom. The activation energies are 3.9 kcal/mol (Pd), 51.0 kcal/mol (Be), 76.7 kcal/mol (Mg), 51.7 kcal/mol (Ca), 91.6 kcal/mol (Zn) and 96.1 kcal/mol (Cd, see Table 1). Thus, the transition metal Pd has by far the lowest barrier followed, with significantly higher barriers, by the alkaline earths and, finally, the group-12 transition metals. All TS structures have C_s point-group symmetry and are characterized by an elongation of the activated C–H bond. The trend in C–H bond elongation along the various metals

roughly reflects the trend in activation energies: it varies from +0.520 Å (Pd), to +0.499, +1.092 and +0.863 Å (Be, Mg and Ca) to +1.225 and +1.355 Å (Zn, Cd, see Fig. 2). This corresponds to percentage-wise elongations of 46–124%. In case of the transition states of Mg (**4b**), Zn (**6b**) and Cd (**7b**), the methyl group has, in addition, considerably flattened and is tilted with respect to the elongated C–H bond (Fig. 2). In all transition states (**3b**–**7b**) except that of Pd (**2b**), the methyl group is staggered with respect to the metal. In the TS of Pd (**2b**) it is eclipsed. These differences are however not that significant. The essential physics is that the methyl group in these structures is virtually a free internal rotor with a rotation barrier in the order of a few tenths of a kcal/mol [10]. Later on, in Section 3.2, we will see that the above trends in activation energy and C–H bond elongation are related in a straight-

forward manner to the valence configuration of the metal atoms.

Similar trends are found for the activation energies and TS structures for oxidative insertion into the chloromethane C–Cl bond. These activation energies relative to reactants are −0.6 (Pd), 24.6 (Mg), 44.3 (Zn) and 46.0 kcal/mol (Cd, see Table 1). Again, the transition metal Pd has by far the lowest barrier followed, with significantly higher barriers, by the alkaline earth Mg and the group-12 transition metals. All TS structures have C_s point-group symmetry and are characterized by an elongation of the activated C–Cl bond. Also, the trend in C–Cl bond elongation along the various metals again roughly reflects the trend in activation energies: it varies from +0.228 (Pd), to +0.807 (Mg) to +0.714 (Zn) and +0.812 Å (Cd) (see Fig. 3 and Table 2). This corresponds to percentage-wise elongations

Table 2
Analysis of the activation energies for Pd, Be, Mg, Ca, Zn, and Cd induced activation of the C–H bond of CH_4 and the C–Cl bond of CH_3Cl in terms of the Activation Strain model

	C–H						C–Cl			
	Pd	Be	Mg	Ca	Zn	Cd	Pd	Mg	Zn	Cd
Energy decomposition (in kcal/mol)										
$\Delta E^{\neq}$	3.9	51.0	76.7	51.7	91.6	96.1	−0.6	24.6	44.3	46.0
$\Delta E^{\neq}_{strain}$	52.2	42.2	105.0	74.6	117.6	122.3	9.9	39.7	40.4	46.0
$\Delta E^{\neq}_{int}$	−48.3	8.8	−28.3	−23.0	−26.0	−26.2	−10.5	−15.2	3.8	0.0
ΔE_{Pauli}	201.7	251.9	98.1	164.9	101.2	86.6	113.4	106.3	95.7	83.2
ΔV_{elst}	−159.1	−108.6	−47.9	−83.5	−55.4	−50.8	−77.8	−68.9	−52.1	−46.2
ΔE_{oi}	−90.9	−134.5	−78.7	−104.4	−71.8	−62.0	−46.1	−52.5	−39.7	−37.0
$\Delta E_{oi}(A')$	−88.1	−126.2	−75.8	−100.5	−70.2	−60.8	−41.8	−49.5	−38.0	−35.5
$\Delta E_{oi}(A'')$	−2.8	−8.2	−2.8	−3.9	−1.7	−1.3	−4.3	−3.0	−1.7	−1.5
C–X bond elongation in TS										
$\Delta(C–X)^{\neq}$ (in Å)	0.520	0.499	1.092	0.863	1.225	1.355	0.228	0.807	0.714	0.812
$\Delta(C–X)^{\neq}$ (in %)	47	46	100	79	112	124	12	44	39	44
Fragment orbital overlap ⟨metal|substrate⟩ in A′ symmetry[a]										
⟨HOMO|HOMO⟩	0.16	0.28	0.24	0.31	0.27	0.25	0.14	0.26	0.18	0.17
⟨HOMO|LUMO⟩	0.22	0.36	0.35	0.25	0.37	0.35	0.04	0.07	0.08	0.08
⟨LUMO|HOMO−1⟩	0.02	0.18	0.25	0.15	0.28	0.26	0.07	0.22	0.27	0.27
⟨LUMO|HOMO⟩	0.39	0.52	0.49	0.26	0.45	0.30	0.18	0.21	0.27	0.26
Fragment orbital population (in electrons) in A′ symmetry[b]										
Metal HOMO	5.38	1.13	1.29	0.89	1.49	1.49	5.63	1.33	1.60	1.56
LUMO	0.42	0.40	0.29	0.52	0.32	0.28	0.22	0.20	0.24	0.22
Substrate HOMO−1	1.99	1.80	1.91	1.90	1.93	1.95	1.97	1.91	1.87	1.88
HOMO	1.66	1.80	1.78	1.72	1.75	1.78	1.86	1.78	1.81	1.82
LUMO	0.34	0.63	0.74	0.84	0.57	0.56	0.21	0.71	0.53	0.57
Fragment orbital energies (in eV) in A′ symmetry										
Metal HOMO−1[c]	−51.3	−106.9[d]	−46.5	−27.7	−10.0	−11.5	−51.3	−46.5	−10.0	−11.50
HOMO[c]	−4.0	−5.5	−4.6	−3.6	−5.9	−5.6	−4.0	−4.6	−5.9	−5.6
LUMO[c]	−3.4	−1.9	−1.0	−1.7	−0.0	−0.2	−3.4	−1.0	−0.0	−0.2
Substrate HOMO−1	−9.9	−9.7	−10.3	−9.8	−10.7	−10.8	−9.1[e]	−7.7[e]	−7.9[e]	−7.7[e]
HOMO	−7.2[e]	−7.6[e]	−6.0[e]	−7.0[e]	−5.7[e]	−5.6[e]	−6.8[f]	−6.4[f]	−6.6[f]	−6.5[f]
LUMO	−1.5[g]	−1.1[g]	−4.0[g]	−2.7[g]	−4.4[g]	−4.6[g]	−2.4[g]	−4.8[g]	−4.7[g]	−5.0[g]

[a] For d (or p) orbitals, overlap values refer to the square root of the combined squares of overlaps of the three (or two) A′-symmetric d (or p) AOs.
[b] For d (or p) orbitals, populations refer to the combined populations of the three (or two) A′-symmetric d (or p) AOs.
[c] HOMO−1, HOMO, LUMO correspond to: 4p, 4d, 5s for Pd; 1s, 2s, 2p for Be; 2p, 3s, 3p for Mg; 3p, 4s, 3d for Ca; 3d, 4s, 4p for Zn; 4d, 5s, 5p for Cd.
[d] The HOMO−1 of beryllium refers to its 1s orbital, which is part of the frozen core (see Section 2.1). For the value of the orbital energy here, a calculation without a frozen core on Be was performed.
[e] $\sigma_{C–X}$.
[f] Cl-lone pair.
[g] $\sigma^*_{C–X}$.

of 12–44%. Note that the elongation of the C–Cl bond in the TS (12–44%) is significantly lower than that of the C–H bond (46–124%) (see Table 2). This contributes to the lower activation energies for insertion into C–Cl as compared to C–H. Furthermore, the transition states come again in two kinds regarding the conformation of the methyl group: staggered relative to the metal (**11b** and **12b**) and eclipsed (**9b** and **10b**, see Fig. 3). However, as pointed out above, these differences are not to be overrated because the methyl group in these structures is virtually a free internal rotor [10].

In conclusion, the transition metal Pd is indeed intrinsically (i.e., already as isolated atom, in the absence of environment effects) more reactive towards oxidative insertion into a C–X bond than alkaline earths and group-12 transition metals. This trend perfectly agrees with condensed-phase experiments despite the obvious modifications of the exact shape of the PES due to solvent and ligand effects. In the following section, we try to find out *why* Pd inserts more readily.

3.2. Activation Strain analysis of reactivity

The results of the Activation Strain analysis are listed in Table 2 and Figs. 5 and 6. Our aim is to elucidate the factors that determine the major trends in our model oxidative-insertion reactions: (i) the increase of the activation barrier from insertion into C–H to C–Cl; and (ii) the increase of the activation barrier from Pd to the alkaline earths to the group-12 transition metals.

Our analyses reveal that the higher activation energies for insertion into the C–H bond originate from the fact that the C–H bond is stronger than the C–Cl bond, 109.7 versus 82.1 kcal/mol at ZORA-BLYP/TZ2P, in line with previous studies [7,25]. To understand this, we analyze the energy profile $\Delta E(\zeta)$ for the reaction of Pd + CH$_3$Cl in terms of the interplay between strain energy $\Delta E_{\text{strain}}(\zeta)$ of the reactants and their mutual interaction energy $\Delta E_{\text{int}}(\zeta)$ along the reaction coordinate ζ [7,25]. The analysis of the energy profile of Pd + CH$_3$Cl is schematically depicted in Fig. 5 (black curves). The strain energy $\Delta E_{\text{strain}}(\zeta)$ increases along the reaction coordinate ζ because the C–Cl bond of the substrate is stretched while the Pd–substrate interaction $\Delta E_{\text{int}}(\zeta)$ becomes more stabilizing due to the decreasing HOMO–LUMO gap of the deformed substrate. The net result is the reaction profile of ΔE with the transition state indicated by a bullet. Note that the reaction coordinate can be represented as the extent of stretching of the C–Cl bond. Now, we switch from the chloromethane C–Cl to the stronger methane C–H bond (not shown in Fig. 5). The main effect is that the $\Delta E_{\text{strain}}(\zeta)$ curve for C–H is destabilized relative to that for C–Cl: it increases more steeply along ζ and achieves a higher final value at the product side than the $\Delta E_{\text{strain}}(\zeta)$ curve for C–Cl. Consequently, also the net energy profile $\Delta E(\zeta) = \Delta E_{\text{strain}}(\zeta) + \Delta E_{\text{int}}(\zeta)$ of the Pd + CH$_4$ reaction is destabilized. Of course, the interaction between reactants $\Delta E_{\text{int}}(\zeta)$ is not completely unaffected by going from C–Cl to C–H. However, the weakening in $\Delta E_{\text{int}}(\zeta)$ that occurs does not change the essence of the above picture. In fact, it somewhat amplifies the effects originating from the strain energy $\Delta E_{\text{strain}}(\zeta)$.

Finally, we address the issue as to *why* the transition metal Pd has *intrinsically* a better capability of inserting into C–X bonds than alkaline earths and group-12 transition metals. We begin with an inspection of the frontier-orbital levels of our series of metal atoms, which are shown in Fig. 6, together with the frontier-orbital levels of methane and chloromethane. Numerical values of the orbital energies can be found in Table 2. There is a number of striking differences between the categories of metals. In the first place, the HOMO–LUMO gap increases from only 0.6 eV for Pd to 1.9–3.6 for the alkaline earths to 5.4–5.9 eV for group 12. This translates directly into a decrease in bonding capabilities along the series because a lower-energy HOMO is a worse electron donor (it has a larger gap with the substrate $\sigma^*_{\text{C–X}}$ acceptor), and a higher-energy LUMO a worse electron acceptor (it has a larger gap with the substrate HOMO, see Fig. 6). This nicely agrees with the computed trend in activation energies which increase in the same order as the bonding capabilities of the metal decrease (see Table 2).

However, the above-discussed trend of decreasing bonding capabilities and increasing Pauli repulsion along Pd,
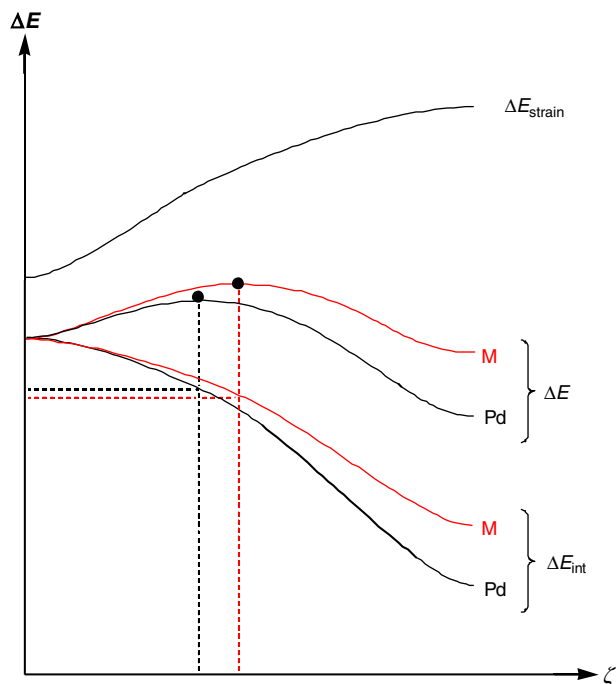

Fig. 5. Schematic potential energy surface ΔE for oxidative insertion and its decomposition into strain energy ΔE_{strain} of and interaction energy ΔE_{int} between substrate and catalyst. The TS (●) is destabilized and shifts forward along the reaction coordinate ζ, towards the product if one goes from Pd (black curves) to a metal M that has poorer bonding capabilities (red curves). (For interpretation of the references to color in this figure legend, the reader is referred to the web version of this article.)
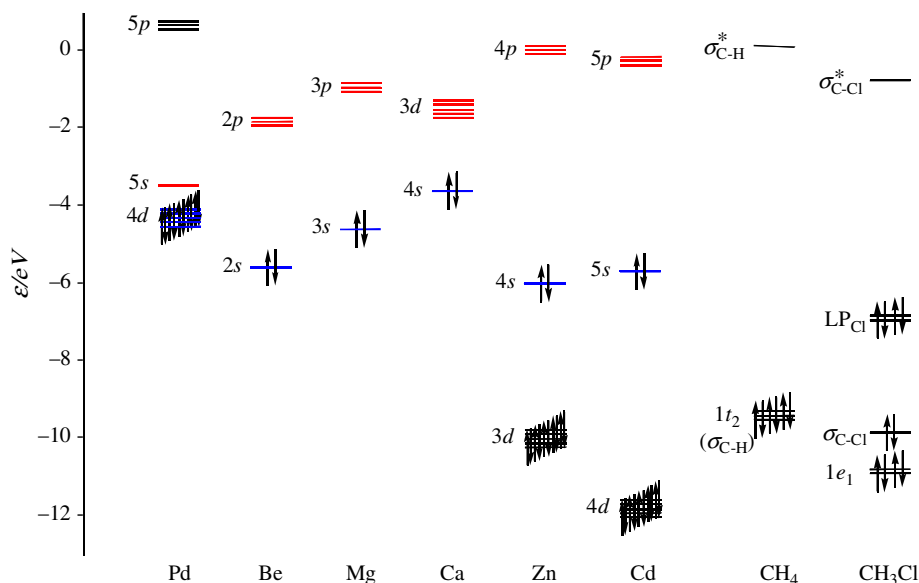
Fig. 6. Frontier orbital levels ε with occupations of Pd, Be, Mg, Ca, Zn Cd, CH_4 and CH_3Cl.

alkaline earths and group-12 atoms seems, at first sight, to be not confirmed by the Activation Strain analyses. In the case of oxidative insertion into the C–H bond, the TS interaction $\Delta E_{int}^{\neq}$ between metal and substrate does weaken from Pd (-48 kcal/mol) to the other metals (-28 to $+9$ kcal/mol) but along the latter (Be, Mg, Ca, Zn and Cd) there is no correlation with the HOMO–LUMO gap of the metal. In the case of oxidative insertion into the C–Cl bond, the TS interaction $\Delta E_{int}^{\neq}$ becomes even *more stabilizing* from Pd (-11 kcal/mol) to Mg (-15 kcal/mol). It is the increase in activation strain $\Delta E_{strain}^{\neq}$ along Pd, alkaline earths and group-12 metals that causes the steady increase in overall barrier along these categories of metals.

Nevertheless, this can all be traced to the decrease in bonding capabilities from Pd to alkaline earths to group 12. We recall that the energy profile (ΔE) for the reactions arises from an interplay of strain energy $\Delta E_{strain}(\zeta)$ of the reactants and their mutual interaction energy $\Delta E_{int}(\zeta)$ [7,25]. The analysis of the energy profile of Pd + CH_3Cl is schematically depicted in Fig. 5 (black curves). As pointed out above, the strain energy $\Delta E_{strain}(\zeta)$ increases along the reaction coordinate ζ because the C–Cl bond of the substrate is stretched while the Pd–substrate interaction $\Delta E_{int}(\zeta)$ becomes more stabilizing due to the decreasing HOMO–LUMO gap of the deformed substrate. The net result is the reaction profile of ΔE with the transition state indicated by a bullet. We also recall that the reaction coordinate can be represented as the extent of stretching of the C–Cl bond. Now, we switch from Pd to the alkaline earths M. This time, the strain curve $\Delta E_{strain}(\zeta)$ is in approximation unaffected. The main effect is that $\Delta E_{int}(\zeta)$ of the alkaline earth metal (red curve) is less stabilizing and descends initially less steeply along ζ than the $\Delta E_{int}(\zeta)$ curve for Pd (in black), see Fig. 5. As a result, also the net energy profile $\Delta E(\zeta)$ of the M + CH_3Cl reaction is destabilized and, because $\Delta E_{int}(\zeta)$ descends *less* steeply, the maximum of

$\Delta E(\zeta)$ shifts to the right, i.e., the TS becomes more product-like. This is why the C–Cl bond expands more in the transition states involving alkaline earths and group-12 metals (i.e., by 39–44%) than in the TS involving Pd (only 12%, see Table 2). Interestingly, the more pronounced C–Cl bond expansion in the TS of Mg causes the corresponding TS interaction $\Delta E_{int}^{\neq}$ to become even more stabilizing than that for Pd. The dashed lines in Fig. 5 illustrate the situation. Thus, the less stabilizing TS interaction $\Delta E_{int}^{\neq}$ occurs not because Pd has worse bonding capabilities. Rather, it occurs because of its *better* bonding capabilities, which make that the TS is reached in an early stage along the reaction coordinate: at that point, the C–Cl bond is less expanded and has therefore a larger HOMO–LUMO gap and, thus, poorer bonding capabilities (mainly poorer electron-acceptor capabilities). A similar mechanism causes the methane C–H bond to expand more in the TS for the oxidative insertion if we go from Pd (0.520 Å) to the alkaline earths (0.499–1.092 Å) to group 12 (1.225–1.355 Å) even though the bonding capabilities decrease along this series of metals (see Table 2 and Figs. 5 and 6).

Of course, the bonding capabilities of metals and substrates are not only determined by orbital energy differences. The latter set a trend in the metal–substrate interactions but this trend can be much affected by the shape of the orbitals (through the resulting overlap) and also by electrostatic interactions. The precise role of these factors has not been resolved here. This requires an extensive exploration and detailed analysis of all terms along a well defined reaction coordinate (e.g., the path of steepest descend from TS to RC) which is however beyond the scope of this pilot study.

In conclusion, the fact that the transition metal Pd is a better agent for oxidative insertion than alkaline earths or group-12 metals can be mainly ascribed to its excellent electron-donating and accepting capabilities associated

with the high-energy 4d HOMO and low-energy 5s LUMO. Together, this causes a more stabilizing palladium–substrate interaction $\Delta E_{int}(\zeta)$ at any point along the reaction coordinate ζ and therefore a lower barrier. The more stabilizing $\Delta E_{int}(\zeta)$ can be masked by the fact that it also causes the TS to shift along ζ towards the reactant-side ("to the left" in Fig. 5) making, on one hand, the TS interaction $\Delta E_{int}^{\neq}$ less *stabilizing* but, on the other hand, the activation strain $\Delta E_{strain}^{\neq} = \Delta E_{strain}(\zeta^{TS})$ less *destabilizing* (see Fig. 5).

4. Conclusions

The transition metal Pd is indeed intrinsically (i.e., already as isolated atom, in the absence of environment effects) more reactive towards oxidative insertion into a C–X bond than alkaline earths and group-12 transition metals. This can be mainly ascribed to palladium's excellent electron-donating and accepting capabilities associated with the high-energy 4d HOMO and low-energy 5s LUMO. Together, this causes a more stabilizing palladium–substrate interaction $\Delta E_{int}(\zeta)$ at any point along the reaction coordinate ζ and therefore a lower barrier as follows directly from our Activation Strain analysis of reactivity, in which the activation energy $\Delta E^{\neq}$ arises as the sum of activation strain $\Delta E_{strain}^{\neq}$ of and TS interaction $\Delta E_{int}^{\neq}$ between metal and substrate: $\Delta E^{\neq} = \Delta E_{strain}^{\neq} + \Delta E_{int}^{\neq}$.

In other words, the high-energy of the Pd 4d HOMO makes the transition metal a good electron donor, which promotes the electronic oxidation process that leads to bond breaking. On the other hand, the low-energy Pd 5s LUMO makes the transition metal a good electron acceptor. This promotes metal–adduct bonding.

Our study focuses on a selection of representative metals (Pd, Be, Mg, Ca, Zn and Cd) and bonds (H_3C–H and H_3C–Cl) that we explored at ZORA-BLYP/TZ2P. Rather than providing a complete sweep through the periodic table, it is a pilot from which one can proceed in various directions. We expect that the main features that make Pd a superior agent in oxidative addition also hold for other transition metals up till group 10 (e.g., Ni and Pt) and that they are passed through also to the corresponding, catalytically active coordination complexes (e.g., ML_2). These expectations are awaiting computational verification.

Acknowledgments

References

[1] V.V. Grushin, H. Alper, Chem. Rev. 94 (1994) 1047;
C. Amatore, A. Jutand, Acc. Chem. Res. 33 (2000) 314.
[2] T.-Y. Luh, M.-K. Leung, K.T. Wong, Chem. Rev. 100 (2000) 3187.
[3] D. Ritter, J.C. Weisshaar, J. Am. Chem. Soc. 112 (1990) 6425;
P. Fayet, A. Kaldor, D.M. Cox, J. Chem. Phys. 92 (1990) 254;
J.J. Carroll, J.C. Weisshaar, J. Am. Chem. Soc. 115 (1993) 800;
A.L. Casado, P. Espinet, Organometallics 17 (1998) 954;
R. Stürmer, Angew. Chem. 111 (1999) 3509;
R.Z. Hinrichs, J.J. Schroden, H.F. Davis, J. Am. Chem. Soc. 125 (2003) 860;
B.C. de Pater, E.J. Zijp, H.-W. Frühauf, J.M. Ernsting, C.J. Elsevier, K. Vrieze, Organometallics 23 (2004) 269;
P. Espinet, A. Echavarren, Angew. Chem. 116 (2004) 4808;
G. Wang, M. Chen, M. Zhou, Chem. Phys. Lett. 412 (2005) 46;
M. Lersch, M. Tilset, Chem. Rev. 105 (2005) 2471.
[4] J.C. Weisshaar, Acc. Chem. Res. 26 (1993) 213;
J.J. Carroll, K.L. Haug, J.C. Weisshaar, M.R.A. Blomberg, P.E.M. Siegbahn, M. Svensson, J. Phys. Chem. 99 (1995) 13955;
M. Porembski, J.C. Weisshaar, J. Phys. Chem. A 104 (2000) 1524;
A. Haynes, P.M. Maitlis, G.E. Morris, G.J. Sunley, H. Adams, P.W. Badger, C.M. Bowers, D.B. Cook, P.I.P. Elliott, T. Ghaffar, H. Green, T.R. Griffin, M. Payne, J.M. Pearson, M.J. Taylor, P.W. Vickers, R.J. Watt, J. Am. Chem. Soc. 126 (2004) 2847.
[5] P.E.M. Siegbahn, M.R.A. Blomberg, M. Svensson, J. Am. Chem. Soc. 115 (1993) 1952;
T.R. Griffin, D.B. Cook, A. Haynes, J.M. Pearson, D. Monti, G.E. Morris, J. Am. Chem. Soc. 118 (1996) 3029;
P.E.M. Siegbahn, J. Am. Chem. Soc. 118 (1996) 1487;
A.M.C. Wittborn, M. Costas, M.R.A. Blomberg, P.E.M. Siegbahn, J. Chem. Phys. 107 (1997) 4318;
Q. Cui, D.G. Musaev, K. Morokuma, J. Chem. Phys. 108 (1998) 8418;
M. Torrent, M. Solà, G. Frenking, Chem. Rev. 100 (2000) 439;
H.M. Senn, T. Ziegler, Organometallics 23 (2004) 2980;
L.J. Gooßen, D. Koley, H. Hermann, W. Thiel, Chem. Commun. (2004) 2141;
S. Kozuch, S. Shaik, A. Jutand, C. Amatore, Chem. Eur. J. 10 (2004) 3072;
G.Th. de Jong, M. Solà, L. Visscher, F.M. Bickelhaupt, J. Chem. Phys. 121 (2004) 9982;
A. Diefenbach, F.M. Bickelhaupt, J. Organomet. Chem. 690 (2005) 2191.
[6] A. Diefenbach, F.M. Bickelhaupt, J. Chem. Phys. 115 (2001) 4030;
A. Diefenbach, G.Th. de Jong, F.M. Bickelhaupt, Mol. Phys. 103 (2005) 995.
[7] A. Diefenbach, G.Th. de Jong, F.M. Bickelhaupt, J. Chem. Theory Comput. 1 (2005) 286.
[8] G.Th. de Jong, D.P. Geerke, A. Diefenbach, F.M. Bickelhaupt, Chem. Phys. 313 (2005) 261.
[9] G.Th. de Jong, D.P. Geerke, A. Diefenbach, M. Solà, F.M. Bickelhaupt, J. Comput. Chem. 26 (2005) 1006;
G.Th. de Jong, F.M. Bickelhaupt, J. Phys. Chem. A 109 (2005) 9685.
[10] G.Th. de Jong, F.M. Bickelhaupt, J. Chem. Theory Comput. 2 (2006) 322.
[11] J.P. Collman, L.S. Hegedus, J.R. Norton, R.G. Finke, Principles and Applications of Organotransition Metal Chemistry, University Science Books, Mill Valley, CA, 1987;
A. Dedieu, Chem. Rev. 100 (2000) 543;
K.C. Nicolaou, P.G. Bulger, D. Sarlah, Angew. Chem. 117 (2005) 4516.
[12] Ch.A. Elschenbroich, A. Salzer, Organometallics: A Concise Introduction, VCH, Weinheim, 1992.
[13] J. March, Advanced Organic Chemistry, McGraw-Hill, Tokyo, 1977.
[14] P. Knochel, J.J. Almena Perea, P. Jones, Tetrahedron 54 (1998) 8275.
[15] K.P.C. Vollhardt, N.E. Schore, Organic Chemistry, W.H. Freeman and Company, New York, 1994.
[16] P.S. Skell, J.E. Girard, J. Am. Chem. Soc. 94 (1972) 5518;
A.W. Ehlers, G.P.M. van Klink, M.J. van Eis, F. Bickelhaupt, P.H.J. Nederkoorn, K. Lammertsma, J. Mol. Model. 6 (2000) 186.
[17] F.M. Bickelhaupt, J. Comput. Chem. 20 (1999) 114.

[18] P. Hohenberg, W. Kohn, Phys. Rev. 136 (1964) B864;
W. Kohn, L.J. Sham, Phys. Rev. 140 (1965) A1133;
R.G. Parr, W. Yang, Density-Functional Theory of Atoms and Molecules, Oxford University Press, New York, 1989.

[19] E.J. Baerends, D.E. Ellis, P. Ros, Chem. Phys. 2 (1973) 41.

[20] G. te Velde, F.M. Bickelhaupt, E.J. Baerends, C. Fonseca Guerra, S.J.A. van Gisbergen, J.G. Snijders, T. Ziegler, J. Comput. Chem. 22 (2001) 931;
E.J. Baerends et al., Computer Code ADF2002.03, SCM, Theoretical Chemistry, Vrije Universiteit, Amsterdam, The Netherlands, 2002.

[21] A.D. Becke, Phys. Rev. A 38 (1988) 3098;
C. Lee, W. Yang, R.G. Parr, Phys. Rev. B 37 (1988) 785.

[22] E. van Lenthe, E.J. Baerends, J.G. Snijders, J. Chem. Phys. 101 (1994) 9783.

[23] E.J. Baerends, O.V. Gritsenko, J. Phys. Chem. A 101 (1997) 5383;
F.M. Bickelhaupt, E.J. Baerends, in: K.B. Lipkowitz, D.B. Boyd (Eds.), Reviews in Computational Chemistry, vol. 15, VCH Publishers, Inc., New York, 2000, p. 1.

[24] T. Ziegler, A. Rauk, Theor. Chim. Acta 46 (1977) 1;
T. Ziegler, A. Rauk, Inorg. Chem. 18 (1979) 1558.

[25] A. Diefenbach, F.M. Bickelhaupt, J. Phys. Chem. A 108 (2004) 8460.